(This is a sample cover image for this issue. The actual cover is not yet available at this time.)

Remote Sensing of Environment 125 (2012) 1–9

Contents lists available at SciVerse ScienceDirect

Remote Sensing of Environment

journal homepage: www.elsevier.com/locate/rse

Correction of MODIS surface reflectance time series for BRDF effects

François-Marie Bréon [a,*], Eric Vermote [b]

[a] Laboratoire des Sciences du Climat et de l'Environnement, Unité Mixte de Recherche CEA-CNRS-UVSQ, 91191 Gif sur Yvette, France
[b] Department of Geographical Sciences, University of Maryland, College Park MD 20742, United States

ARTICLE INFO

Article history:
Received 20 December 2011
Received in revised form 26 June 2012
Accepted 27 June 2012
Available online xxxx

Keywords:
Surface reflectance
BRDF
MODIS
Directional effects

ABSTRACT

Surface reflectance time series measured from space borne instruments, such as the MODIS sensor, show an apparent high-frequency noise that limits their information content. A major contributor to this noise is the directional effect as the target reflectance varies with the observation geometry. The operational MODIS processing inverts the parameters of a BRDF model which are provided in the so-called MCD43C2 product with a frequency of $(8\ \text{days})^{-1}$. Recently, Vermote et al. (2009) suggested an alternative BRDF inversion method. A major assumption is that the BRDF model shape (i.e. the BRDF normalized by its overall amplitude) varies little throughout the year so that the two model parameters are linear functions of the NDVI. Consequently, a given target BRDF shape is described by four parameters (slope and intercept for the two NDVI-dependent parameters) rather than 2 parameters that change for each 8 days period. This method imposes additional constrain for the surface BRDF inversion.

In this paper, we evaluate the performance of these two approaches for the correction of surface reflectance time series. We work at the 0.05° (≈5 km) resolution of the CMG grid and analyze a representative set of +100 targets selected on the basis of the location of AERONET sites. The performance is quantified by the high-frequency noise in the corrected time series. We demonstrate that the performances of the two approaches are very similar. This result demonstrates that a simple four-parameter NDVI-scaled model performs as well as a more complex model with many more degrees of freedom. Besides, the four-parameter model, which is inverted on a given year, can be applied to the measurements of other years with a similar level of performance. Finally, a single "averaged" model can be applied to any target with a performance that is only slightly reduced compared to what is achieved with a model derived through a full inversion of the multi-temporal data.

The proposed four-parameter BRDF model permits the reduction of noise in the reflectance time series by a factor of the order of three in the red and four in the near infrared. After correction, the reflectance time series are very clean, with an apparent noise that is ≈0.005 in the red band and 0.01 in the near infrared. The quality of the BRDF correction makes it possible to use the individual reflectance time-series at high temporal resolution, rather than indices based on their ratio, and thus retain more information about the vegetation dynamics.

1. Introduction

It is now more than ten years since the MODIS (MODerate resolution Imaging Spectrometer) instruments on-board Terra and Aqua are providing a daily near-complete view of the Earth. The measurements from these instruments allow countless applications from climate studies, from crop-yield prediction to disaster monitoring. One such application is the monitoring of vegetation coverage and dynamics. Indeed, the red and Near Infrared (NIR) channels at 250 m resolution (bands 1 and 2) are used to identify the presence of vegetation and to quantify its photosynthetic activity. The fraction of sunlight reflected by the surface depends on the surface cover. Vegetation reflectance is high in the NIR, while chlorophyll absorption makes it much lower in the visible.

Surface reflectance time series from the MODIS sensors, but also from other imaging instruments such as VGT (Maisongrande et al., 2004) or MERIS (Bezy et al., 2000), can then be used to follow the vegetation cycle and to identify inter-annual anomalies. There are a number of difficulties that affect the quantitative use of the space borne measurements. One is the calibration, another one is the correction of the atmospheric effects (Vermote et al., 2009), while the one discussed in this paper is the correction of directional effects. Indeed, the reflectance of an Earth target varies strongly with the observation geometry (both sun and view directions). The maximum reflectance is commonly observed in the backscatter direction (view and sun directions coincide) with a sharp increase within a few degrees (Breon et al., 2002). Conversely, the minimum reflectance is generally observed in the forward direction, and this minimum is

* Corresponding author. Tel.: +33 169089455; fax: +33 169087716.
E-mail address: fmbreon@cea.fr (F.-M. Bréon).

0034-4257/$ – see front matter © 2012 Elsevier Inc. All rights reserved.
doi:10.1016/j.rse.2012.06.025

over a very broad range of view directions. The ratio of maximum to minimum reflectance can be up to 5 in the red and 3 in the NIR (Breon et al., 2002). One option, to limit the impact of directional effect, is to use only those observations that are close to nadir viewing. This is a serious limitation as it strongly reduces the number of usable observations. Besides, it does not correct for the impact of sun angle variations. Another option is to use so called vegetation indices such as the NDVI (Normalized Difference Vegetation Index, (Tucker, 1979)) or the EVI (Enhanced Vegetation Index, (Huete et al., 2002)). Indeed, as the directional signatures are similar in the red and NIR bands, reflectance ratios or any index based on reflectance ratios, are less sensitive to directional effect than individual reflectances. However, there are still significant directional signatures in the vegetation indices (Sims et al., 2011). In addition, some information on the vegetation change is lost in the use of ratios compared to the original reflectances (Baret & Guyot, 1991). The reflectance variations in the various spectral bands contain some information about the vegetation structure and leaf pigments that is lost in the vegetation index (Houborg et al., 2007). It is then desirable to correct the directional effects in the measured reflectance time series.

The reflectance variation with the viewing geometry are quantified by the Bidirectional Reflectance Distribution Function (BRDF) that is a function of the sun zenith angle θ_s, the view zenith angle θ_v and the relative azimuth angle ϕ. We implicitly assume that the target has no preferred direction so that only the relative azimuth, and not both the sun and view azimuth, intervenes in the BRDF.

The purpose of this paper is to quantitatively evaluate three methods for the correction of directional signature effects in reflectance time series. The first method uses the official MODIS BRDF product that is derived from the measurements of both MODIS/Terra and MODIS/Aqua over a period of 16 days (Schaaf et al., 2002). An alternative method uses a model that is inverted from the measurements acquired over a full year, assuming that the target BRDF shows limited changes that are linked to the NDVI (Vermote et al., 2009). Finally, we also evaluate the performance of the correction model with a single set of parameters, representative of all snow-free land surfaces.

Section 2 presents the data and methods used in this paper. Section 3 shows the results; section 4 discusses the results and concludes.

2. Data and method

2.1. Parametric BRDF models

A practical inversion of reflectance measurements in terms of BRDF parameters, suitable for directional effect correction, necessitates the use of analytical models. Although several authors favour the use of non-linear BRDF models, such as RPV (Rahman et al., 1993) (Lavergne et al., 2007), linear models are widely used to fit a set of reflectance measurements. Indeed, (Maignan et al., 2004) shows that a linear model matches a set of multi-directional reflectance measurements from the space borne POLDER instrument with a similar quality as RPV does, and even better on average.

Widely used linear BRDF models compute the reflectance ρ as the sum of three terms (Roujean et al., 1992):

$$\begin{aligned}\rho(\theta_s,\theta_v,\phi) &= k_0 + k_1 F_1(\theta_s,\theta_v,\phi) + k_2 F_2(\theta_s,\theta_v,\phi)\\ &= k_0\left[1 + \frac{k_1}{k_0}F_1(\theta_s,\theta_v,\phi) + \frac{k_2}{k_0}F_2(\theta_s,\theta_v,\phi)\right]\end{aligned} \quad (1)$$

where F_1 is the volume scattering kernel, based on the Ross-Thick function and F_2 is the geometric kernel. F_1 is a semi-physical function that attempts to reproduce the BRDF of a thick vegetation layer. F_2 is also based on physical consideration, but for hypothetical surface with protrusions. F_1 and F_2 are fixed functions of the observation geometry, but k_0, k_1 and k_2 are free parameters. In the following, we will use V (for *Volume*) as k_1/k_0 and R (for *Roughness*) as k_2/k_0.

The operational processing of MODIS to compute surface BRDF and Albedo is based on this three-parameter linear model with the Ross-Thick and Li-Sparse kernels (Schaaf et al., 2002). The analysis of POLDER multidirectional measurements against several BRDF models (Maignan et al., 2004) has shown that a slightly better fit to space borne measurements could be obtained through a correction of the Ross-Thick function (F_1) to account for the so-called Hot-Spot effect (Breon et al., 2002). This model correction is only significant when the observation geometry is close to the backscatter direction, which is seldom sampled by passive sensors. Nevertheless, we recommend the use of a corrected version of the Ross-Thick function F_1 as in (Maignan et al., 2004) for a better representation of the directional signature close to backscatter and also to allow comparisons with active sensing that is sensitive to the BRDF in the exact backscatter direction.

The correction of the directional effects is done by putting the measurement in a standard observation geometry. In the following, the standard observation geometry is for a sun at 45° from zenith and the observation at nadir. This is an arbitrary choice, but it is a typical geometry for space borne remote sensing and is not affected by the strong directional signature close to backscatter. The normalized reflectance, ρ^N, is therefore computed as:

$$\rho^N(45,0,0) = \rho(\theta_s,\theta_v,\phi)\frac{1 + VF_1(45,0,0) + RF_2(45,0,0)}{1 + VF_1(\theta_s,\theta_v,\phi) + RF_2(\theta_s,\theta_v,\phi)} \quad (2)$$

In the following text, for simplicity and efficiency of writing, the N superscript always refers to the standard observation geometry and we drop the explicit notation to θ_s, θ_v and ϕ. Eq. (2) becomes:

$$\rho^N = \rho\frac{1 + VF_1^N + RF_2^N}{1 + VF_1 + RF_2} \quad (3)$$

2.2. MODIS reflectance

Our analysis is focused on MODIS bands 1 (red: 620–670 nm) and 2 (NIR: 841–876 nm). These bands are the most widely used for land surface monitoring and they cover a wide range of reflectance over vegetated surfaces. The original measurements have a nominal spatial resolution of 250 m for those channels, although it degrades with the view angle. For practical purposes of data volume, and also to limit the noise induced by the increase in pixel size at large view angles (Wolfe et al., 1998), the present study uses data aggregated at the lower (0.05°, ≈5 km) resolution of the CMG grid (Climate Modelling Grid). This grid is used for a number of MODIS products, including the MCD43C2 product that provides BRDF parameters and Albedo for snow-free conditions at the global scale. We have averaged the original measurements at 250 m resolution within the corresponding CMG pixel. We use both MODIS/Aqua and MODIS/Terra measurements indiscriminately. The analysis shown below is primarily based on the measurements acquired during 2003, although we also processed the measurements of 2004 and 2005 to analyze the BRDF shape variability. The original 250 m measurements were extracted from the MOD09 surface reflectance product (Vermote et al., 2002; Vermote & Kotchenova, 2008) that is corrected for the atmospheric effect (molecular and aerosol scattering and absorption, ozone and water vapour absorption). The data were also filtered for cloud, cloud shadow and snow according to the internal quality flags provided in the MOD09 product. For a consistent analysis of multi-temporal data, we only kept the CMG observation if all high-resolution pixels were clear.

2.3. Selected sites

Our analysis uses a set of representative land surface targets. The selection is based on the location of the stations of the AERONET (AErosol RObotic NETwork) sun photometer network (aeronet.gsfc.nasa.gov). A few stations are located on a coastline and the corresponding pixel contains a large fraction of water. In such cases (i.e. when the water fraction is larger than 15%), rather than using the CMG pixel that contains the sun photometer station, we use the adjacent pixel containing the least water. After this adjustment, 5 stations, all located on islands, were still contaminated by a large fraction of water and were eliminated from our selection. In addition, we selected only the pixels with more than 70 MODIS measurements during the year, including both Terra and Aqua. From the original set of 140 AERONET stations, we retained 115. The sites locations are shown in Fig. 1 and listed in Table 3 of the Supplementary material. Although not homogeneously distributed, this selection covers a wide range of surface types and geometries of observation.

2.4. MCD43C2 product

The MCD43C2 product provides the 3 k_i BRDF parameters (Eq. (1)) for the red and NIR bands, together with the Albedo and results for other spectral bands. This product is given at the CMG resolution and is therefore compatible with the surface reflectances we aggregated. We have verified that the MCD43C2 product is consistent with the result of our averaging at 0.05° from the original 250 m reflectances, i.e. that the spatial structures of the two are highly correlated, indicating that we did not introduce any spatial shift. The MCD43C2 product is provided at a temporal resolution of 8 days, but is derived from a combination of Aqua and Terra measurements over a 16 days period. The method for the BRDF model inversion is described in (Schaaf et al., 2002). In Fig. 3, left, three examples of time series of the BRDF parameter ratios (i.e. $V=k_1/k_0$, $R=k_2/k_0$) are shown. V and R follow an annual cycle that is likely the result of the growth and senescence of vegetation. However, the model parameters also exhibit significant high-frequency variability that is unrealistic and probably result from instabilities in the inversion procedure or noise in the input reflectances (Ju et al., 2010).

2.5. Alternative model

An alternative method was proposed in (Vermote et al., 2009), hereafter referred to as VJB. There are three main hypothesis in this method: (i) the target BRDF can be represented with a linear model as in Eq. (1); (ii) the model parameters V and R vary linearly with the NDVI over the full year; and (iii) the normalized reflectance, e.g. $k_0(t)$, varies slowly so that its variation between three successive measurements is linear in time. A minimization of the high frequency variations of the BRDF-corrected reflectance is used to invert the model parameters independently for the different spectral bands. One major difference with the MODIS BRDF product (MCD43C2) is that a full year of measurements is used to invert the model, instead of a 16 days period. In Fig. 3, left panel, the R and V parameters for 3 sites selected among those in our study are shown as symbols. There is less high-frequency variability than with the official product (lines) but this cannot be used as an indication of robustness as the two parameters are linear function of the NDVI so that their short-term variability is directly linked to that of the vegetation index.

The retrieved R has a similar order of magnitude for MCD43 and VJB. We recall that the F_1 functions are not exactly the same for the two correction methods but the differences are only significant in a viewing geometry close to backscatter, so that the k_i parameters are directly comparable. It is interesting to note that the two methods show similar annual cycles for V and R, despite the high frequency temporal variations in the MCD43C2 results.

One may question the use of the NDVI as a proxy to quantify the BRDF signature. In addition, other vegetation indices have been proposed and show better performance for some applications. The primary reason for using the NDVI is that BRDF have been shown to be significantly different for bare soil and vegetated surfaces, because vegetated surfaces show higher anisotropy than bare soil do (Bacour & Breon, 2005). The NDVI is a parameter that is sensitive to the presence of vegetation, and easy to derive from the measurements that we seek to correct. However, although the NDVI is much less sensitive to directional effects than the reflectances are, there is still some directional signature that translates into noise on the NDVI, and therefore R and V. One way to (partly) account for this noise is to compute a NDVI from the original measurements, estimate the BRDF model (R and V), correct the reflectance measurements, compute a corrected NDVI, and make a new estimate of R and V that shall be less sensitive to NDVI changes. This iterative procedure was *not* applied for the results presented here.

2.6. Averaged model

Fig. 2 shows R and V for the 115 selected sites. There are four plots that correspond to the two bands and the two (R and V) parameters, which are shown as a function of NDVI. Each segment corresponds to one target site. The X-axis range of each segment corresponds to the

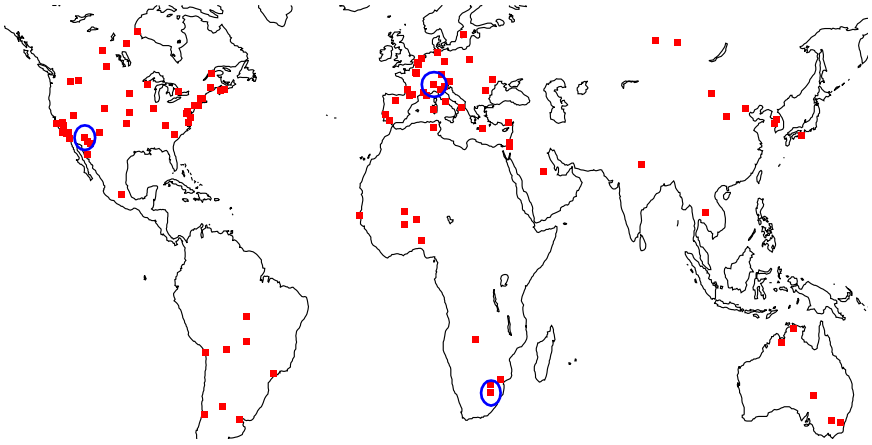

Fig. 1. Location of the targets used in this paper for BRDF evaluation. The selection was based on the location of AERONET sites. For a few sites located along the coast (i.e. when the fraction of land within the corresponding CMG pixel is less than 85%) we selected the adjacent pixel with the largest land fraction. The circles highlight the three sites that are shown in Fig. 3.

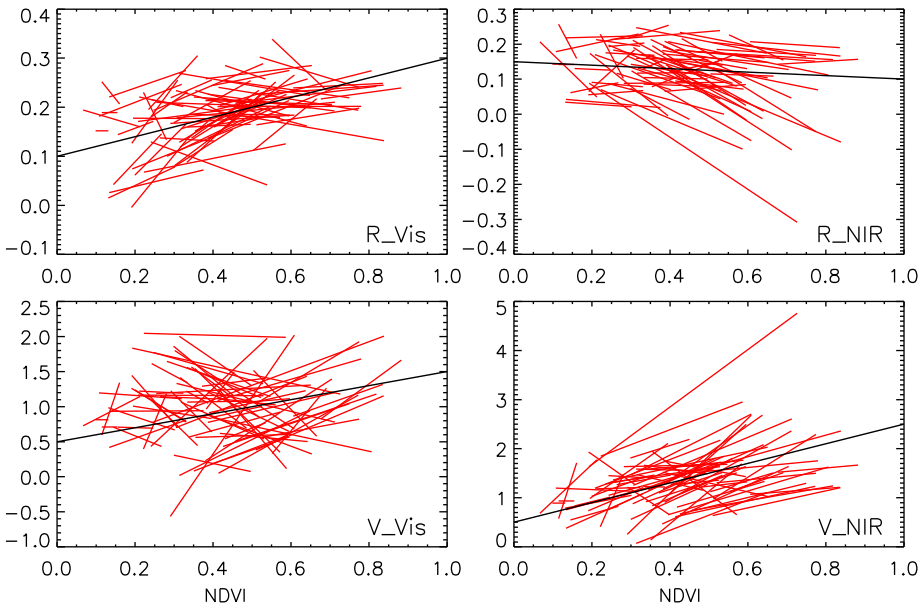

Fig. 2. R (top) and V (bottom) parameters as a function of NDVI for the sites analyzed in this paper. Red (channel 1) is on the left while Near Infrared (channel 2) is on the right. Each line segment corresponds to one site and is drawn using the corresponding NDVI variability for this site. The thick black line indicates the "averaged" model.

range of NDVI during the year for that particular target (at 5% and 95% of the measurements cumulative histogram). The Y-axis values are then computed from the slope and intercept values of the respective parameters:

$$R = R_{slope} NDVI + R_{intercept}$$
$$V = V_{slope} NDVI + V_{intercept} \quad (4)$$

On the one hand, there is significant variability of the BRDF parameters among the sites as shown in Fig. 2. On the other hand, the mean value of each parameter is significantly different than zero. Besides, there is a general trend with the NDVI, at the very least for R_{vis} and V_{nir}. These observations suggest the definition of an "averaged" model for V and R, represented by a black line in Fig. 2. The slopes and intercept values that define this "averaged" model are provided in Table 1. One question that is discussed in the following is whether this model, which would only be a function of the local NDVI, can be used for the correction of directional signatures in reflectance time series. Fig. 2 shows that there is significant variability around the mean so that the BRDF variability is not a sole function of the NDVI. Thus, the question is: what fraction of the BRDF-induced "noise" can be corrected by the "averaged" model? and what is the residual noise when using such correction?

2.7. Evaluation method

To quantify the impact of the correction on the reflectances or the vegetation indices, we compute an estimate of the noise. This estimate assumes a linear variation of the reflectance between two dates a few days apart. Given three successive reflectance measurements, the two extremes can then be used to estimate a reflectance value for the one in the middle:

$$R_i^* = \frac{(\mathrm{day}_i - \mathrm{day}_{i-1}) R_{i+1} + (\mathrm{day}_{i+1} - \mathrm{day}_i) R_{i-1}}{\mathrm{day}_{i+1} - \mathrm{day}_{i-1}} \quad (5)$$

An error is computed from the difference of this estimate with the actual measurement (either corrected or not). For a set of N observations during the year, there is N − 2 such triplets that are used to compute a statistical noise:

$$\sigma^2(R) = \frac{\sum_{i=2}^{N-1} \frac{1}{\mathrm{day}_{i+1} - \mathrm{day}_{i-1}} (R_i^* - R_i)^2}{\sum_{i=2}^{N-1} \frac{1}{\mathrm{day}_{i+1} - \mathrm{day}_{i-1}}} \quad (6)$$

The reasoning that leads to this expression for the quantification of the noise is detailed in the appendix. Note that the weighting by $(day_{i+1} - day_{i-1})^{-1}$ gives less weight to the measurements triplets that are distant in time. We make this choice as non-linear variations of the reflectance with time may be expected for long time periods. Fig. 3, right, shows several reflectance time series and provide σ for each of them (numbers within the plots). The values of σ are consistent with the visual quality of the different time series.

Eqs. (5) and (6) provide an objective method for assessing the quality of a BRDF correction. Clearly, the BRDF "noise" is not the sole contributor to σ. Other contributors are atmospheric correction errors, measurement noise, and non-linear reflectance temporal variations. However, these are the same for all BRDF correction methods so that the value of σ may be used to compare and rank the performance of several methods.

One may ask what is the relationship between σ and the noise of individual measurements. Let us assume that the measurements, either before or after directional correction, are affected by a purely random -uncorrelated- noise ε. We acknowledge that this is not fully true as there may be some correlated error as a result of directional effects, or biases in the directional correction. The relationship between σ and ε also depends on the distribution of the time intervals. If we assume that there is an independent measurement every day, then $\sigma = \sqrt{3/2}\,\varepsilon$. At the other extreme, if there are very few measurements randomly distributed, then $\sigma = \sqrt{5/3}\,\varepsilon$. A rather

Table 1
Typical values for the slope and intercept that define V and R as a function of the NDVI (see Eq. (4) and Fig. 2).

	R		V	
	Slope	Intercept	Slope	Intercept
Band 1 (Vis)	0.2	0.1	1	0.5
Band 2 (NIR)	−0.05	0.15	2	0.5

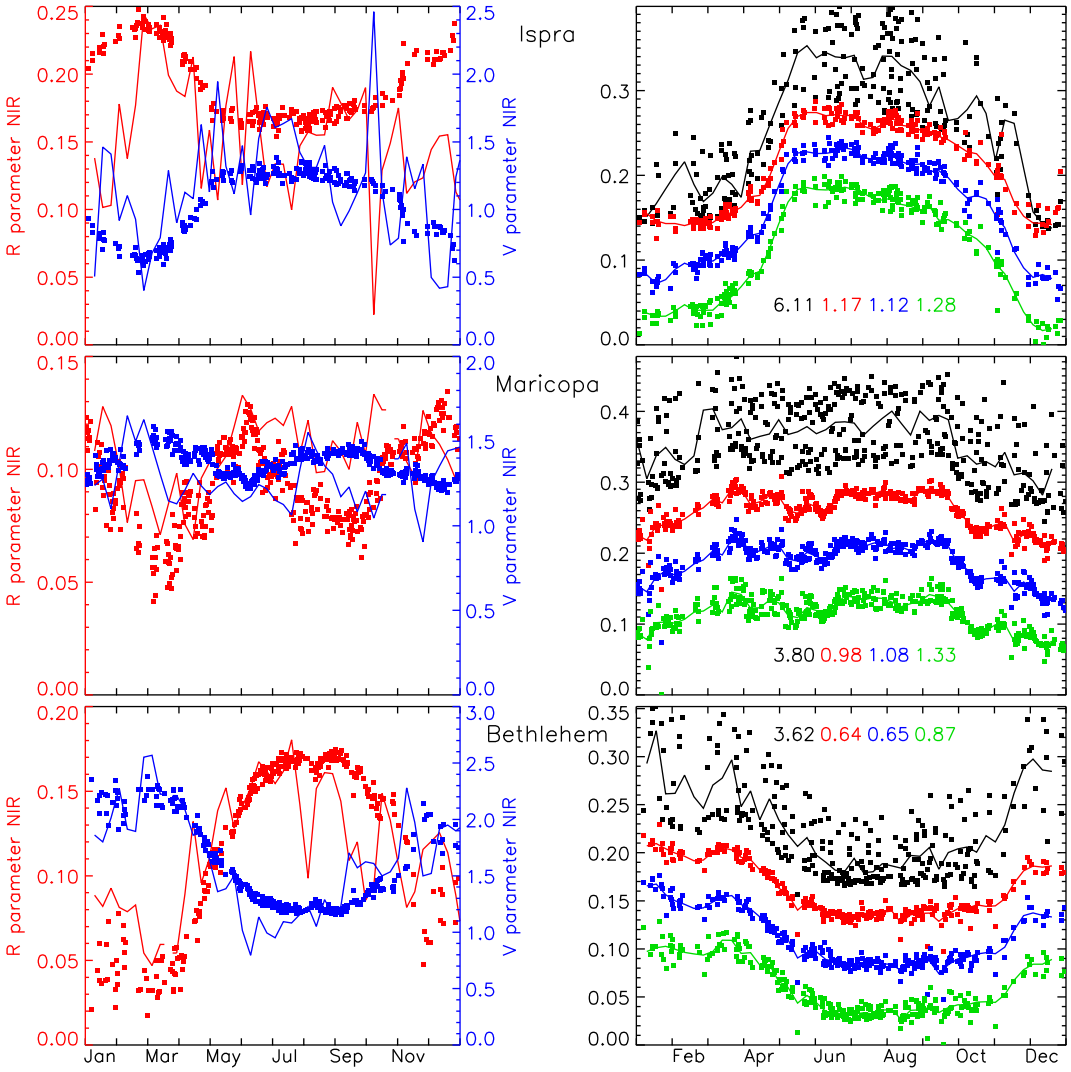

Fig. 3. Time series of R and V BRDF parameters (left) and near infrared (MODIS band 2) reflectance (right). The BRDF parameters (left column) are shown for both MCD43C2 MODIS product (line) and for the result of the VJB method (dots). The surface reflectance time series (right column) are shown for the original measurements (black), after VJB correction (red), after MCD43C2 model correction (blue) and for the averaged model correction (green). The lines show a simple temporal fit through the data points. The original measurements (black) are the actual values, but the corrected reflectances have been shifted by 0.05 (red), 0.1 (blue) and 0.15 (green). The numbers in the right plots are the temporal noise σ [$\times$100] as defined in Eq. (6) with matching colors. The selected sites are Ispra (Forest/urban), Maricopa (Crops/Desert), and Bethlehem (Crops). For interpretation of the references to color in this figure legend, the reader is referred to the web version of this article.

good approximation is therefore $\sigma \approx 1.25\ \varepsilon$. These results derive from a simple statistical analysis of Eqs. (5) and (6).

3. Results

3.1. BRDF parameter variability

Fig. 3 (left) shows three examples of BRDF parameters variability. The lines show the MODIS official product (MCD43C2) while the dots correspond to the VJB method. As said above, the variability in the VJB parameters (R and V) are directly linked to NDVI variability. Its relative stability throughout the year is therefore imposed by the method. On the other hand, the MCD43C2 parameters show significant high frequency variability. One does not expect the surface to change significantly between the 16 days periods with such large impacts on the BRDF parameters (Quaife & Lewis, 2010). Some of the variations in R and V are anti-correlated (see in particular the large swings for the Ispra site, top). These variations can be explained by the fact that, for some observation geometry configurations, *F1* and *F2* are far from orthogonal or, in other words, highly correlated, so that the inversion of their respective parameters is poorly constrained. But in some cases, a large variation in R (resp. V) is not linked to a similar variation in V (resp. R) (see for instance a large short-term drop of R early August for the Bethlehem site).

Fig. 3 only shows results for band 2 (NIR) but similar results have been analyzed for band 1. For the latter, the high-frequency variations of MCD43C2 parameters that we interpret as noise are more pronounced than for band 2 while the noise in the VJB parameters is not substantially different than for band 2.

3.2. Reflectance time series

Fig. 3 (right) shows three examples of reflectance time series. The black dots are the original measurements. Red, blue and green are the same measurements after correction by VJB model, MCD43C2 model, and "averaged" model respectively. The numbers provide the high-frequency noise (see Eq. (6)) expressed $\times$100. The lines are the results of a smoothing interpolation through the data points. Clearly, all three BRDF models allow an excellent correction of the high-frequency noise in the measurements. This confirms, if needed, that the dominant contributor to the noise in the reflectance time series is the directional effect. After correction, one can depict temporal

signatures in the reflectances that are undistinguishable from the noise in the original time series. On these figures, none of the three BRDF correction methods performs significantly better than the others although the quantitative indicator is somewhat consistently larger (and therefore not as good) for the "averaged" model. Clearly, there is a need for a larger dataset to state whether one method is better than another.

Note that the large swings on the MCD43C2 parameters do not have a discernable impact on the reflectance time series. There are a few measurements that appear clearly anomalous through each correction method (see for instance a few points that are clearly below all their neighbours in the right-bottom plot of Fig. 3). These probably result from an undetected shadow or an error in the atmospheric correction. Such measurements should be eliminated from the time series when analyzing the surface dynamic, and their identification is clearly much easier after directional correction than before. The "averaged" model does not need any data inversion or extraneous information, and is therefore well suited for that purpose.

3.3. Correction performance

Fig. 4 shows scatter plots of the apparent noise σ ($\times 100$) (see Eq. (6)) for the various correction methods. The X-axis is the result of the VJB method, while the Y-axis is, from top to bottom, the original measurements, the measurements corrected using the MCD43C2 parameters, the "averaged" model method, and VJB method but using the retrieved coefficients from another year (2005 coefficients to correct 2003 measurements). The left (right) column is for the red (NIR) band. The top plots confirm that the original time series are always much noisier than their corrected counterparts. The other plots indicate that the three methods have similar performances. The variability between sites is much larger than the differences between the correction methods. This indicates that the residuals of the BRDF correction are small compared to the other sources of error. For the "averaged" model (third line from top), most points are above the 1:1 line, which indicates that it does not perform as well as the VJB correction. Nevertheless, the performance of this "averaged" model appears adequate for most sites. Some applications may want to trade accuracy for simplicity and use the "averaged" model (Table 1) for a BRDF correction that applies to all pixels, bare soils or vegetated.

Conversely, the points on both lower plots are very much aligned around the 1:1 line. This shows that the VJB model parameters that are inverted from the measurements of a given year (here 2005) can be used to correct the measurements of another year. This result opens the way for a near real-time correction where the inverted BRDF parameters from the previous year (or another) are used to correct the measurements for directional effects.

Fig. 5 provides another presentation of the relative performance of the various model corrections. Each line shows a cumulative histogram of σ ($\times 100$) (see Eq. (6)). The X axis has a logarithmic scale to better depict the differences for the low values (best targets). These figures confirm previous results: all correction methods allow a large reduction in apparent noise in the time series. The averaged model has slightly less good performances than the others. There is no significant difference between VJB and MCD43C2, although the former appears slightly better (cumulative histogram to the left), in particular for the lower range of values. One may argue that these correspond to the "best" targets where the contributions of noise factors other than the directional effects are smallest. Only for such targets does the impact of the small difference between BRDF models become apparent. A similar observation was made in (Maignan et al., 2004).

Table 2 provides typical values for the apparent noise ($\times 100$) in the time series for the non-corrected measurements as well as for the various correction methods. We provide the median value, as well as a typical value for the "best" targets, i.e. the value at 20% of the cumulative histogram of Fig. 5. The table provides quantitative values from the curves of Fig. 5 and quantifies the performances of the various methods. Table 3, in Supplementary material, provides the noise for each method and each of the targets used in this paper. Before the directional correction, the typical noise in the reflectance time series is close to 0.02 in the red and 0.04 in the near-infrared. After the correction, the typical noise is 0.006 in the red and close to 0.01 in the near-infrared. Overall, the typical reduction of noise is a factor of 3 in the red and 4 in the NIR. Table 2 shows that this ratio is the same for the best quality targets.

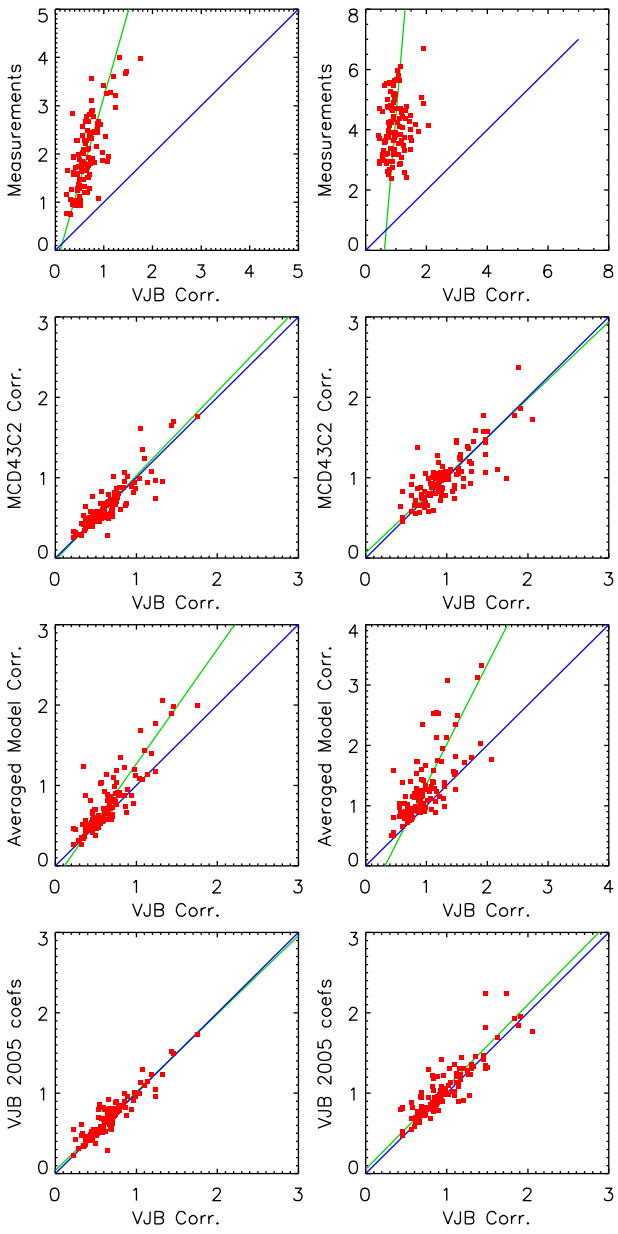

Fig. 4. Scatter plot of the apparent noise σ ($\times 100$) of the reflectance and corrected reflectance time series (see Eq. (6)). Left is for the red (band 1), while right is for the near infrared (band 2). The two lines are the 1:1 line and the best fit among the data points.

4. Discussion and conclusion

In this paper, we have compared the performances of several methods to correct the directional effects in reflectance time series

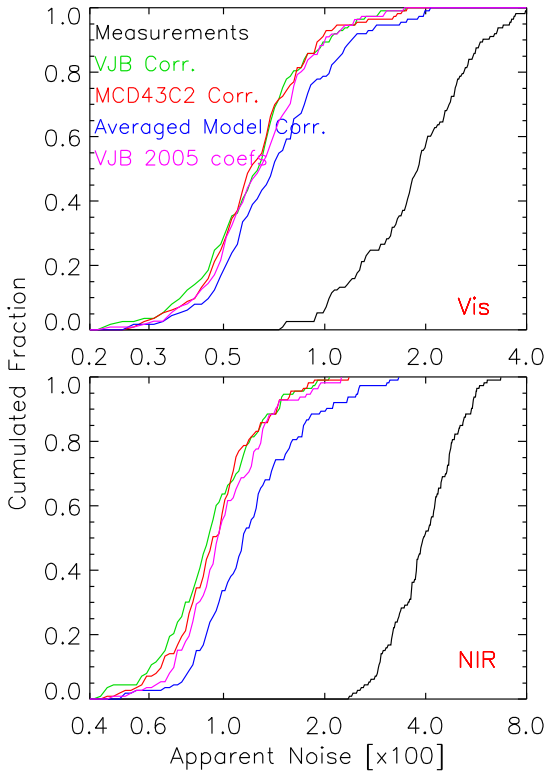

Fig. 5. Cumulative histogram of the apparent noise of the reflectance and corrected reflectance time series. Top is red (band 1) whereas bottom is Near InfraRed (band 2).

acquired by the MODIS instruments. All methods extrapolate the measurement to a standard geometry using a BRDF model. The major difference between the official method and that of VJB is that the former derives a different model for each 16 day periods, while the latter hypothesizes that the two model parameters are linear functions of the NDVI. As a consequence, the description of a target BRDF for a full year (and even multiple years as was shown above) is achieved through four parameters per spectral band, while the same with the official model requires two parameters per period. Clearly, using the VJB correction method is more practical as it requires much fewer inputs. Using fewer parameters also leads to a better-constrained inversion, with less instability in the results (see Fig. 3 left). The results have shown that the two methods have a similar performance for the correction of reflectance time series. An interesting result is that, for a given target, the VJB coefficients of a given year apply to the correction of measurements from another year. The quality of the BRDF correction does not make it necessary to use ratio-based vegetation indices such as the Normalized Difference Vegetation Index (Tucker, 1979) or the Simple Ratio, and thus retain more information about the surface.

Table 2
Typical noise (×100) for the reflectance time series in the red and Near Infrared bands for the original data and the various directional corrections. The values are extracted from Fig. 5 and show the median noise (i.e. value at 50% of the cumulative histogram), as well as the typical noise for the "best" targets (i.e. value at 20% of the cumulative histogram).

	Red		Near infrared	
	20% histo	Median	20% histo	Median
Measurements	1.26	1.88	3.18	3.94
VJB Corr.	0.44	0.62	0.70	0.90
MCD43C2 Corr	0.46	0.60	0.76	0.96
"Averaged" model	0.50	0.68	0.88	1.14
VJB 2005 Coeffs.	0.48	0.64	0.78	0.96

An important question is whether there is some added information in the high frequency (daily; cloud cover permitting) monitoring of the land surfaces. Indeed, simple low-pass filter through the measured reflectance would retain the annual cycle and remove the high-frequency noise induced by the directional effects. However, the near random sampling (occurrence of cloud cover for instance) may favour some directions during a given period. These directions may lead to a high or low bias in the smoothed values. If one selects only some viewing geometries (such as close to nadir), it may result in no observation during a long period. Thus, it appears desirable to use all available directions and account explicitly for their observation geometry. In addition, a careful analysis of the corrected time series (see Fig. 3) clearly shows short-term features that are probably real and would be smoothed out by a low-pass filter. Some applications, such as the timing of phenology as a response of meteorological forcing (Maignan et al., 2008), analyze signatures with a temporal resolution of one to a few days. Thus, there is certainly information in the daily reflectance time series, even if it has received little attention so far, due to a lack of proper measurement.

The time series of the BRDF parameters in the MCD43C2 product show rather large temporal variations (Fig. 3, left). These are unrealistic and cast doubt on the validity of the BRDF quantified by these parameters. Yet, this paper demonstrates that these parameters allow an accurate correction of the reflectance time series. One may see a contradiction in an apparently very noisy set of BRDF parameters that nevertheless leads to accurate values. The explanation lies in the sampling of the BRDF. During a 16 days period, the MODIS/Aqua and MODIS/Terra instrument provide a limited sample of the BRDF. Within this sample, there is a high correlation between the F_1 and F_2 functions, so that the retrieval of the V and R weights are poorly constrained. However, these parameters allow an excellent fit to the measurements made during the analysis period, and are therefore well suited for their correction. However, the corresponding BRDF does not necessarily apply to measurements acquired with other observation geometries.

Conversely, the BRDF model derived through the VJB method is constrained by a much wider set of observation geometries, and in particular a large range of sun angles as a result of the seasonal change, in addition to the view angle range. A single BRDF model applies for the full year of measurements. This is a strong indication that the model is better constrained and can be used for a wide range of observation geometries.

A significant outcome of this paper is the definition of a "typical" BRDF model that is a function of the NDVI only. This rather simple model might be use for a rough correction of BRDF effects in reflectance time series. Although a full inversion of the BRDF model results in better results, some applications, such as real time processing, may want to trade accuracy for simplicity.

The present study has been performed at the CMG spatial resolution (≈5 km). One may argue that the results are applicable only at this scale while finer scale BRDF are more anisotropic and show more variability so that the simple NDVI-scaled model would not apply. Indeed, airborne measurements have shown that the surface BRDF depends on the spatial scale of the measurements (Roman et al., 2011). However, in our opinion, there is no convincing indication that surface BRDF are more anisotropic at finer scales, or that a simple kernel-based BRDF model does not work at a finer scale than what is used here. Nevertheless, it remains to be verified. This would be relatively easy once the fine scale reflectance time series have been downloaded, together with the result of the official BRDF product. We have started this process and an analysis at the full MODIS resolution will be the subject of a forthcoming paper. We are concerned however that the degradation of the MODIS spatial resolution at large view angle will generate additional noise in the measurements, which will make the comparison of BRDF models more difficult.

Supplementary data to this article can be found online at http://dx.doi.org/10.1016/j.rse.2012.06.025.

Acknowledgments

Three anonymous reviewers provided most useful comments on the submitted version of this paper. We also thank Bernard Pinty and Luigi Boschetti for providing valuable suggestions on an earlier version of the manuscript.

Appendix A. Justification for error quantification

In this Appendix, we explicit the reasoning that leads to the error quantification as in Eq. (6).

The surface reflectance in a standard observation geometry shows a time evolution $R(t)$. The satellite data provide a sampling of this evolution at discrete times t_i. We therefore have to evaluate the accuracy of an ensemble R_i that provides an estimate of R at t_i ($1 \le i \le N$ where N is the number of samples).

Clearly, the best would be to compare the ensemble R_i to the truth and compute an RMS error such as

$$RMS = \sqrt{\frac{1}{N}\sum_{i=1}^{N}(R_i - R(t_i))^2} \qquad (A-1)$$

The trouble is, we have no independent knowledge of $R(t)$ and therefore cannot compute the rmse this way. This is why one needs an alternative. The alternative is to use the hypothesis that $R(t)$ varies slowly in time so that its temporal variation are very close to linear. This assumption can be written mathematically as:

$$R(t_2) = \frac{(t_2-t_1)R(t_3) + (t_3-t_2)R(t_1)}{t_3-t_1} + \delta(t_1,t_2,t_3); \quad |\delta| << |R(t_3)-R(t_1)| \qquad (A-2)$$

In the following, we assume that δ is small compared to the noise in the reflectance estimates and can be neglected. The N values of R_i provide estimates of $R(t_i)$. Then

$$R_i = R(t_i) + \varepsilon \qquad (A-3)$$

We search for the statistical properties of ε. We make the assumption that the ε_i are independent. From the time series of normalized reflectances R_i we can build $(N-2)$ triplets $[R_{i-1}, R_i, R_{i+1}]$. Our quantification of the noise (Eq. (6)) is based on

$$\sigma^2(R) = \frac{\sum_{i=2}^{N-1}\frac{1}{t_{i+1}-t_{i-1}}(R_i^*-R_i)^2}{\sum_{i=2}^{N-1}\frac{1}{t_{i+1}-t_{i-1}}} \qquad (A-4)$$

where

$$R_i^* = \frac{(t_{i+1}-t_i)R_{i-1} + (t_i-t_{i-1})R_{i+1}}{t_{i+1}-t_{i-1}} \qquad (A-5)$$

Substituting R_i as in Eq. (A-3) and using Eq. (A-2) above (neglecting δ), leads to:

$$\sigma^2 = \frac{\sum_{i=2}^{N-1}\frac{1}{(t_{i+1}-t_{i-1})^3}\left((t_{i+1}-t_i)\varepsilon_{i-1} + (t_{i+1}-t_{i-1})\varepsilon_i + (t_i-t_{i-1})\varepsilon_{i+1}\right)^2}{\sum_{i=2}^{N-1}\frac{1}{t_{i+1}-t_{i-1}}} \qquad (A-6)$$

or, with the notation $x_i = \frac{t_{i+1}-t_i}{t_{i+1}-t_{i-1}}$

$$\sigma^2 = \frac{\sum_{i=2}^{N-1}\frac{1}{(t_{i+1}-t_{i-1})}\left(x_i\ \varepsilon_{i-1} + \varepsilon_i + (1-x_i)\varepsilon_{i+1}\right)^2}{\sum_{i=2}^{N-1}\frac{1}{t_{i+1}-t_{i-1}}} \qquad (A-7)$$

We now use the assumptions that the ε_i are uncorrelated with a zero mean. The implication is that the sums $\sum_{i=2}^{N-1}\frac{1}{(t_{i+1}-t_{i-1})}\varepsilon_{i-1}\varepsilon_i$; $\sum_{i=2}^{N-1}\frac{1}{(t_{i+1}-t_{i-1})}\varepsilon_i\varepsilon_{i+1}$; $\sum_{i=2}^{N-1}\frac{1}{(t_{i+1}-t_{i-1})}\varepsilon_{i-1}\varepsilon_{i+1}$ can be neglected. Then:

$$\sigma^2 = \frac{\sum_{i=2}^{N-1}\frac{1}{(t_{i+1}-t_{i-1})}\left(x_i^2\ \varepsilon_{i-1}^2 + \varepsilon_i^2 + (1-x_i)^2\varepsilon_{i+1}^2\right)}{\sum_{i=2}^{N-1}\frac{1}{t_{i+1}-t_{i-1}}} \approx \left(\overline{x^2} + 1 + \frac{\overline{1}}{1-\overline{x^2}}\right)\overline{\varepsilon^2} = 2\left(1-\overline{x}+\overline{x^2}\right)\overline{\varepsilon^2} \qquad (A-8)$$

If the observations are evenly distributed in time, then $x = 0.5$ so that $\sigma^2 \approx 3/2\ \overline{\varepsilon^2}$. For uneven distributions, x can take random values between 0 and 1, so that $\sigma^2 \approx 5/3\ \overline{\varepsilon^2}$.

These equations demonstrate that, as indicated in the main body of the manuscript, σ^2 provides an objective and quantitative evaluation of the statistical difference between the "truth" $R(t)$ and the individual R_i with some clearly stated assumptions.

References

Bacour, C., & Breon, F. M. (2005). Variability of biome reflectance directional signatures as seen by POLDER. *Remote Sensing of Environment*, *98*, 80–95.

Baret, F., & Guyot, G. (1991). Potentials and limits of vegetation indexes for Lai and Apar assessment. *Remote Sensing of Environment*, *35*, 161–173.

Bezy, J. L., Delwart, S., & Rast, M. (2000). MERIS — A new generation of ocean-colour sensor onboard Envisat. *Esa Bulletin-European Space Agency*, 48–56.

Breon, F. M., Maignan, F., Leroy, M., & Grant, I. (2002). Analysis of hot spot directional signatures measured from space. *Journal of Geophysical Research — Atmospheres*, *107*, -, D16.

Houborg, R., Soegaard, H., & Boegh, E. (2007). Combining vegetation index and model inversion methods for the extraction of key vegetation biophysical parameters using Terra and Aqua MODIS reflectance data. *Remote Sensing of Environment*, *106*, 39–58.

Huete, A., Didan, K., Miura, T., Rodriguez, E. P., Gao, X., & Ferreira, L. G. (2002). Overview of the radiometric and biophysical performance of the MODIS vegetation indices. *Remote Sensing of Environment*, *83*, 195–213.

Ju, J. C., Roy, D. P., Shuai, Y. M., & Schaaf, C. (2010). Development of an approach for generation of temporally complete daily nadir MODIS reflectance time series. *Remote Sensing of Environment*, *114*, 1–20.

Lavergne, T., Kaminski, T., Pinty, B., Taberner, M., Gobron, N., Verstraete, M. M., et al. (2007). Application to MISR land products of an RPV model inversion package using adjoint and Hessian codes. *Remote Sensing of Environment*, *107*, 362–375.

Maignan, F., Breon, F. M., & Lacaze, R. (2004). Bidirectional reflectance of Earth targets: Evaluation of analytical models using a large set of spaceborne measurements with emphasis on the Hot Spot. *Remote Sensing of Environment*, *90*, 210–220.

Maignan, F., Breon, F. M., Vermote, E., Ciais, P., & Viovy, N. (2008). Mild winter and spring 2007 over Western Europe led to a widespread early vegetation onset. *Geophysical Research Letters*, *35*, L02404.

Maisongrande, P., Duchemin, B., & Dedieu, G. (2004). VEGETATION/SPOT: An operational mission for the Earth monitoring; presentation of new standard products. *International Journal of Remote Sensing*, *25*, 9–14.

Quaife, T., & Lewis, P. (2010). Temporal constraints on linear BRDF model parameters. *IEEE Transactions on Geoscience and Remote Sensing*, *48*, 2445–2450.

Rahman, H., Verstraete, M. M., & Pinty, B. (1993). Coupled surface-atmosphere reflectance (Csar) Model .1. Model description and inversion on synthetic data. *Journal of Geophysical Research — Atmospheres*, *98*, 20779–20789.

Roman, M. O., Gatebe, C. K., Schaaf, C. B., Poudyal, R., Wang, Z. S., & King, M. D. (2011). Variability in surface BRDF at different spatial scales (30 m–500 m) over a mixed agricultural landscape as retrieved from airborne and satellite spectral measurements. *Remote Sensing of Environment*, *115*, 2184–2203.

Roujean, J. L., Leroy, M., & Deschamps, P. Y. (1992). A bidirectional reflectance model of the earth's surface for the correction of remote-sensing data. *Journal of Geophysical Research — Atmospheres*, *97*, 20455–20468.

Schaaf, C. B., Gao, F., Strahler, A. H., Lucht, W., Li, X. W., Tsang, T., et al. (2002). First operational BRDF, Albedo nadir reflectance products from MODIS. *Remote Sensing of Environment*, *83*, 135–148.

Sims, D. A., Rahman, A. F., Vermote, E. F., & Jiang, Z. N. (2011). Seasonal and inter-annual variation in view angle effects on MODIS vegetation indices at three forest sites. *Remote Sensing of Environment*, *115*, 3112–3120.

Tucker, C. J. (1979). Red and photographic infrared linear combinations for monitoring vegetation. *Remote Sensing of Environment*, *8*, 127–150.

Vermote, E. F., El Saleous, N. Z., & Justice, C. O. (2002). Atmospheric correction of MODIS data in the visible to middle infrared: First results. *Remote Sensing of Environment*, *83*, 97–111.

Vermote, E., Justice, C. O., & Breon, F. M. (2009). Towards a generalized approach for correction of the BRDF effect in MODIS directional reflectances. *IEEE Transactions on Geoscience and Remote Sensing*, *47*, 898–908.

Vermote, E. F., & Kotchenova, S. (2008). Atmospheric correction for the monitoring of land surfaces. *Journal of Geophysical Research — Atmospheres*, *113*, D23.

Wolfe, R. E., Roy, D. P., & Vermote, E. (1998). MODIS land data storage, gridding, and compositing methodology: Level 2 grid. *IEEE Transactions on Geoscience and Remote Sensing*, *36*, 1324–1338.